processes

MDPI

Article

Introducing Non-Hierarchical RSM and MIGA for Performance Prediction and Optimization of a Centrifugal Pump under the Nominal Condition

Wenjie Wang [1,2], Ju Sun [1], Jun Liu [3,*], Jiantao Zhao [1], Ji Pei [1] and Jiabin Wang [3]

[1] National Research Center of Pumps, Jiangsu University, 301 Xuefu Road, Zhenjiang 212013, China
[2] Wenling Research Institute of Fluid Machinery, Jiangsu University, Taizhou 317522, China
[3] Shandong Shuanglun Co., Ltd., Weihai 264203, China
* Correspondence: liujun@shuanglun.cn

Abstract: In order to improve the operation performance of the multi-stage double-suction centrifugal pump and reduce the internal energy loss of the pump, this paper proposes a single-objective optimization design method based on the non-hierarchical response surface methodology (RSM) and the multi-island genetic algorithm (MIGA). Nine parameters, such as the blade outlet width and blade wrap angle, were used as design variables, and the optimization objective was efficiency under design conditions. In total, 149 sets of valid data were obtained under the Latin hypercube sampling method (LHS), the corresponding thresholds were set for efficiency and head, and 99 sets of valid data were obtained. A cross-validation analysis of the sieved data was carried out based on non-hierarchical RSM, global optimization of the efficiency was carried out using MIGA, and numerical verification was carried out via CFD. The research results show that compared with hierarchical RSM, non-hierarchical RSM can approximate the nonlinear relationship between the objective function and the design variables with higher accuracy, and the model fitting R^2 value was 0.919. The efficiency was improved by 3.717% after optimization. The overall prewhirl of the impeller inlet after optimization decreased, the internal speed of the volute significantly improved, the large-area vortex at the volute and the outlet pipe was eliminated, the impact loss at the volute separating tongue disappeared, and the overall hydraulic performance of the pump was improved. The total entropy output value of the optimized pump was reduced by 4.79 (W/K), mainly concentrated on the reduction in the entropy output value of the double volute, and the overall energy dissipation of the pump was reduced.

Keywords: multi-stage double-suction centrifugal pump; non-hierarchical RSM; MIGA; optimization

Citation: Wang, W.; Sun, J.; Liu, J.; Zhao, J.; Pei, J.; Wang, J. Introducing Non-Hierarchical RSM and MIGA for Performance Prediction and Optimization of a Centrifugal Pump under the Nominal Condition. *Processes* **2022**, *10*, 1529. https://doi.org/10.3390/pr10081529

Academic Editor: Cherng-Yuan Lin

Received: 16 July 2022
Accepted: 2 August 2022
Published: 4 August 2022

1. Introduction

As general mechanical equipment in the field of fluid machinery, pumps are widely used in production and in life for the purpose of conveying fluid media. For the multi-stage double-suction centrifugal pumps used in the fields of sewage treatment, water diversion irrigation, and industrial water supply, during the large-flow and high-head operation and due to the complexity of the structure, it is easy to cause an internal flow disorder, which results in the low overall efficiency of the pump [1,2].

However, current pump manufacturers and users have increasingly higher requirements for pump performance, and obtaining a high-efficiency pump type has become essential. In the field of hydraulic machinery, the use of numerical simulation methods to optimize the mechanical properties of pumps has been widely used [3]. Traditional pump design is accomplished via a combination of numerical calculations and experiments; the design process is very complicated, and the calculation process takes a long time. At present, with intelligent optimization algorithms being applied more and more widely, optimization design that combines numerical calculations and an intelligent optimization algorithm is also very common. The operational speed and accuracy of this combination

method are greatly improved as compared with those of the original model. This can reduce the labor and experimental costs, and a better pump model is ensured. Ji et al. [4] proposed to use a radial basis function (RBF) neural network to optimize the impeller of a turbo centrifugal pump, with sampling based on the Latin hypercube sampling (LHS) method; their results showed that the optimized model efficiency and head improved as compared with the original model, at 5.74% and 4.85%, respectively. Chen et al. [5] combined the Kriging model with numerical analysis to find the optimal design parameters for a torque converter impeller, thereby improving the performance of the torque converter. Piri et al. [6] proposed a hybrid analysis framework based on an artificial neural network (ANN) to evaluate the probability of failure of sewage pumping stations; the framework accurately predicted the safety margin of the pump and reduced the computational burden. Nataraj et al. [7] used response surface methodology (RSM) and computational fluid dynamics (CFD) to design an impeller to improve the performance of a centrifugal pump, resulting in a 2.06 m increase in total head and a 65.22 W reduction in power dissipation. Yang et al. [8] used RSM to study and optimize the jet pump, taking the pressure amplitude and the time-averaged power dissipation of a jet pump as responses to achieve maximum pressure amplitude and minimum power consumption. The final results showed that RSM is feasible as an evaluation method for optimizing jet pumps. Alawadhi et al. [9] optimized the efficiency of a pump based on RSM and the multi-objective genetic algorithm, and they used geometric parameters, including the number of blades, impeller speed, etc., as design variables to predict the performance of the pump under stable and transient conditions, and also to predict corrosion. The Kriging model, radial basis neural network, and artificial neural network are generally applicable to occasions with a large sample size, while RSM is suitable for occasions with a small sample size, which can obtain better fitting accuracy and randomness in the case of more design variables being available [10].

RSM was firstly proposed by Box and Wilson; it is a comprehensive test technology that deals with the relationship between input variables and output responses [11]. As a commonly used statistical analysis technique, RSM has the characteristics of strong applicability and wide application range, which enables it to effectively locate the individual effects and interactions between parameters [12]. In an optimization process with many design variables, a high-intensity nonlinear programming is generally used between the objective function and the design variables. At present, most scholars use low-order polynomial functions to fit the objective function. Miletic et al. [13] studied the usefulness of combinations based on RSM and ANN in characterization, modeling, and optimization, and they found better results for the prediction of second-order polynomial functions by comparing the fitted R^2 values of linear and second-order RSM polynomial functions. Wang et al. [14] proposed an optimization strategy for developing a turbine runner model based on CFD technology, a second-order RSM and a multi-objective genetic algorithm. Taking six geometric parameters, such as the blade load, as design variables, some design problems of the turbine runner were effectively solved, and the calculation cost was reduced. Zhang et al. [15] proposed an integrated method based on second-order RSM and the genetic algorithm to analyze the influence of various parameters of the standpipe inlet and outlet and to obtain an optimal design; finally, the total head loss coefficient and the inflow and outflow velocity distribution coefficients were reduced by 4.687%, 11.765%, and 38.596%, respectively. However, compared with low-order polynomial functions, using high-order polynomial functions to fit functions can obtain higher prediction accuracy. In order to obtain more reliable test data for an air source heat pump, Ciarrocchi et al. [16] used fourth-order RSM to expand the data sample; they examined the performance of the air source heat pump by changing the water supply temperature of the indoor terminal under different environmental conditions. An optimal configuration of the system was found, which minimized power consumption while maintaining interior comfort.

We can improve the quality of the higher-order RSM by eliminating unnecessary terms, which also reduces the uncertainty of model prediction and improves the fitting accuracy. This kind of polynomial that randomly ignores some lower-level terms is called

a non-hierarchical polynomial [17]. Bao et al. [18] proposed an efficient stochastic update method based on statistical theory and developed an incomplete fourth-order polynomial RSM. Combining RSM with Monte Carlo Simulation (MCS) reduces computation and enables fast random sampling. Tanaka et al. [19] applied an interactive hierarchical RSM to the parameter optimization of photonic crystal nanocavities, and they demonstrated the effectiveness of this method for parameter optimization.

In summary, although there are many studies on the application of RSM at home and abroad, there are few applications for a complex high-order RSM. In this paper, the efficiency of a multi-stage double-suction centrifugal pump is optimized based on the improved fourth-order non-hierarchical RSM polynomial. The effects of different polynomial terms on the approximate accuracy of RSM are compared. In Section 2, the hydraulic model, mesh generation, and numerical calculations are presented. Then, in Section 3, the optimization objectives, optimization variables, variable ranges, agent model, and the algorithm in the optimization process are described. In Section 4, the sensitivity analysis of each geometric parameter is carried out, and the inner flow state and entropy generation performance of the pump before and after optimization are compared and analyzed. Finally, the conclusion is given in Section 5.

2. Pump Model Parameters and Computational Method

2.1. Hydraulic Model

The first-stage single-suction impeller and the secondary double-suction impeller of the multi-stage double-suction centrifugal pump use the same impeller hydraulic model. In order to better eliminate the radial force of the impeller when the pump is running, the volute of the flow passage adopts a double volute design. At the design operating point, the design performance parameters of the pump are: flowrate Q = 540 m^3/h, design head H = 132 m, speed n = 1490 r/min, and specific speed n_s = 64. The formula for calculating the specific speed is as follows:

$$n_s = \frac{3.65nQ^{1/2}}{H^{3/4}} \quad (1)$$

The overall 3D pump fluid domain was modeled in the model design software UG NX, as shown in Figure 1. After the water enters the suction chambers on both sides, it flows into the middle symmetrical flow channel perpendicular to the axis through the single-suction impellers on both sides. It then flows into the double-suction impeller from the flow channel and finally discharges through the middle-pressure water chamber. The specific details of the flow through the impeller are shown in Figure 2. The main design parameters of the multi-stage double-suction centrifugal pump are shown in Table 1.

Table 1. Main design parameters of the multi-stage double-suction centrifugal pump.

Parameter	Abbreviation	Value
Flow rate	Q	540 m^3/h
Head	H	132 m
Rotating speed	n	1490 r/min
Specific speed	n_s	54.09
Impeller inlet diameter	D_1	196 mm
Impeller outlet diameter	D_2	485 mm
Impeller outlet width	b_2	15 mm
Volute inlet width	b_3	70 mm
Volute inlet diameter	D_3	495 mm
Volute outlet diameter	D_4	200 mm
Number of blades	Z	8

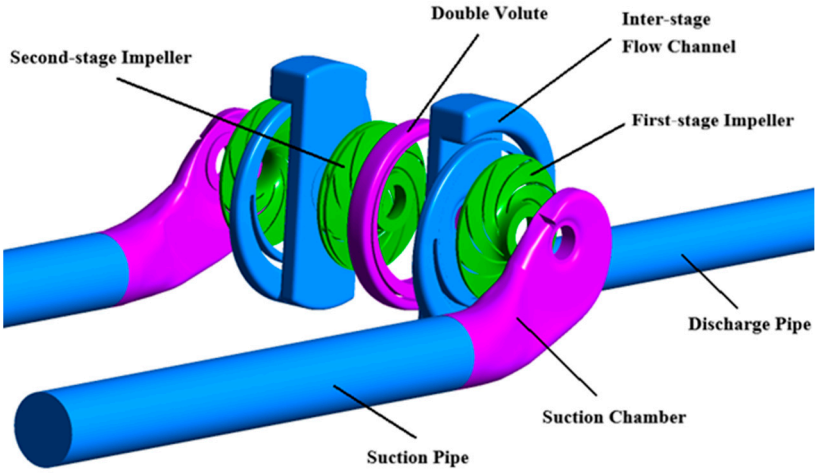

Figure 1. Computational domain of the multi-stage double-suction centrifugal pump.

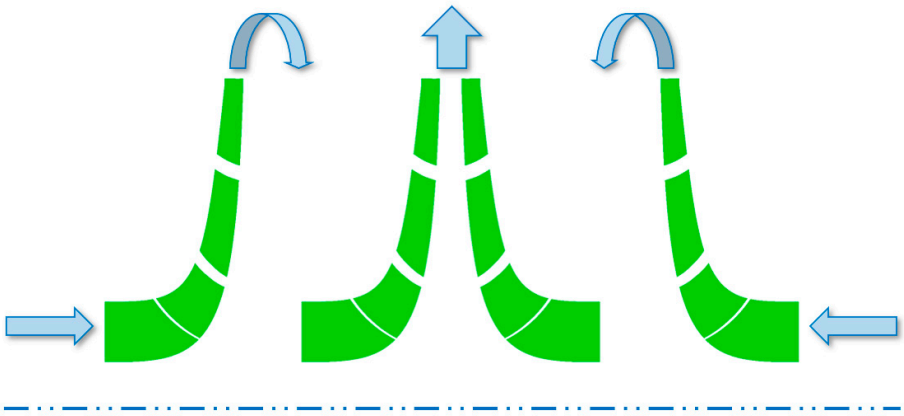

Figure 2. Schematic diagram of water flow through the impeller.

2.2. Mesh Generation and Numerical Calculation

Due to the complexity of the double volute internal structure of the multi-stage double-suction centrifugal pump, ANSYS ICEM was used to generate unstructured meshes. The impeller, suction chamber, interstage runner, and other components were based on the commercial software TurboGrid, which has high precision and good convergence performance in its high-quality structural grid. In order to better satisfy the subsequent high-precision flow field analysis and more accurately characterize the complex flow phenomena around the solid wall, the mesh of the solid surface was refined. Part of the computational domain grid is shown in Figure 3.

The CFD in the commercial software ANSYS CFX was used to study and analyze the hydraulic characteristics of the pump. The turbulence model adopted was the shear stress transfer model (SST k-ω), which is widely used in multi-stage double suction centrifugal pumps and can predict the flow separation and pump performance with good accuracy [20–22]. In order to meet the requirements of the above turbulence model, the maximum y^+ used for the impeller blade was less than 10; Figure 4 shows the contour of y^+.

In the independence analysis of the effect of the number of grid cells on the numerical calculation results, a total of five groups of independent grid numbers were generated; the calculation results of the corresponding lift and efficiency are shown in Table 2. After the grid-independence analysis, the grid size was finally determined. The final number of cells was 130.858×10^5. The total pressure inlet and mass flow outlet were set as the boundary conditions of the pump. The computational domain generated a total of 11 networks, including the suction chamber, suction pipe, first-stage impeller, inter-stage flow channel,

second-stage impeller, double volute, and outlet pipe grid. The number of grid cells for each computational domain is shown in Table 3.

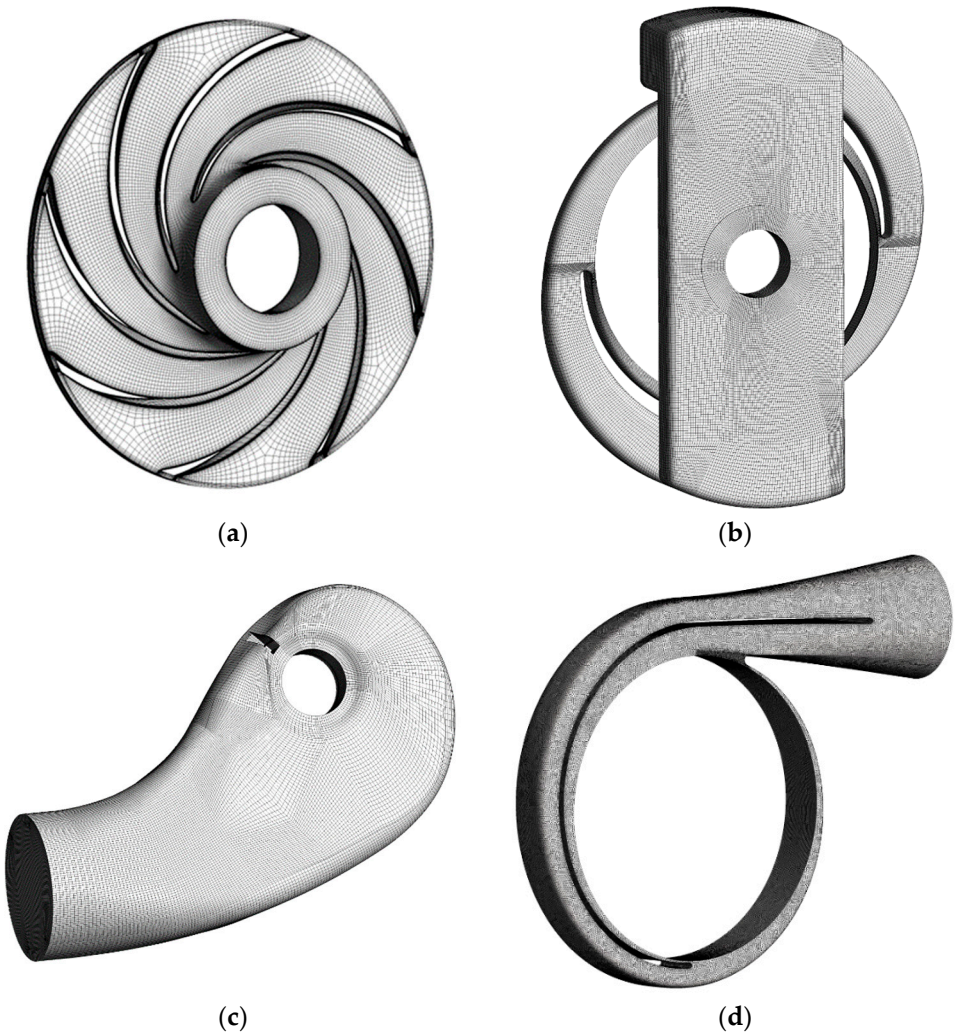

Figure 3. Meshes of the calculation domain: the impeller (**a**), the inter-stage flow channel (**b**), the suction chamber (**c**), and the volute (**d**).

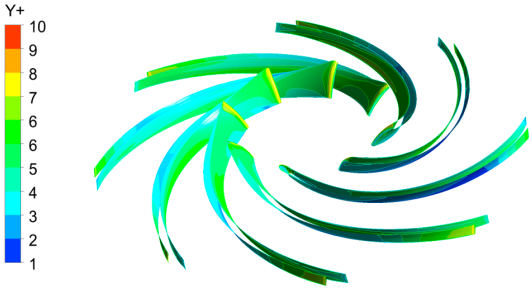

Figure 4. The blade contour of *y*+.

Table 2. Results of the grid independence analysis.

Grid number ($\times 10^5$)	113.236	121.46	130.858	145.749	153.758
Head (m)	129.885	136.956	138.62	135.78	128.875
Efficiency (%)	73.975	75.863	76.512	75.461	73.23

Table 3. The number of grid cells for each computational domain.

Domain	Number of Grid Cells ($\times 10^5$)	Number
Suction pipe	1.67	2
Suction chamber	7.78	2
Impeller	12.45	4
Inter-stage flow channel	12.78	2
Double volute	27.10	1
Discharge pipe	9.48	1

2.3. Experimental Verification

A comparison between the test results and the numerical calculation results is shown in Figure 5. It can be seen from the figure that the trends of the test curve and the numerical calculation curve are almost the same. Since the energy loss generated by the pump itself was not fully considered during the test, the test results for the head and efficiency were generally lower than the numerical calculation results. At the design operating point, the numerical calculation result of the pump was 76.512%, the test result was 73.705%, and the absolute error of the two was 2.807%. Under non-design conditions, the error between the numerical calculation results and the experimental results did not increase greatly, therefore the numerical simulation method in this paper is reliable and can be used for subsequent optimization studies.

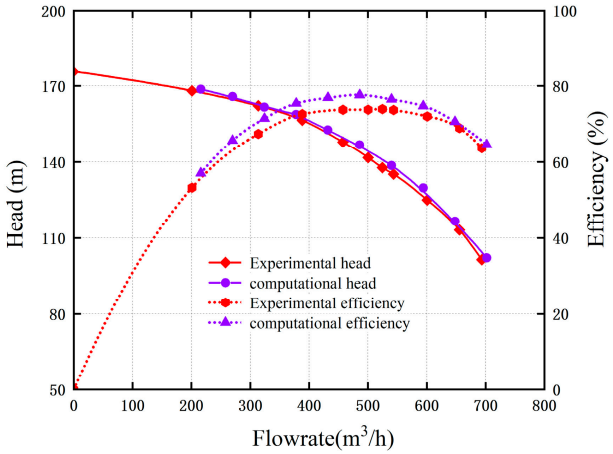

Figure 5. Comparison of experimental results and numerical calculation results.

3. Optimization Process

Figure 6 presents the optimization flow chart for this paper. The efficiency under the design condition of the multi-stage double-suction centrifugal pump was selected as the optimization objective, the nine design parameters of the pump were used as the optimization variables, and respective boundary conditions were set for the nine variables. The Latin hypercube sampling (LHS) method was used to generate 149 groups of valid sample data, the performance of the original scheme was compared, the data were screened, the functional relationship between the objective function and the design variables was established, and the objective function was fitted based on the improved response surface methodology (RSM) using the multi-island genetic algorithm (MIGA). This algorithm finds the optimal efficiency point for CFD verification and finally obtains the optimal geometric parameter design of the volute and the impeller.

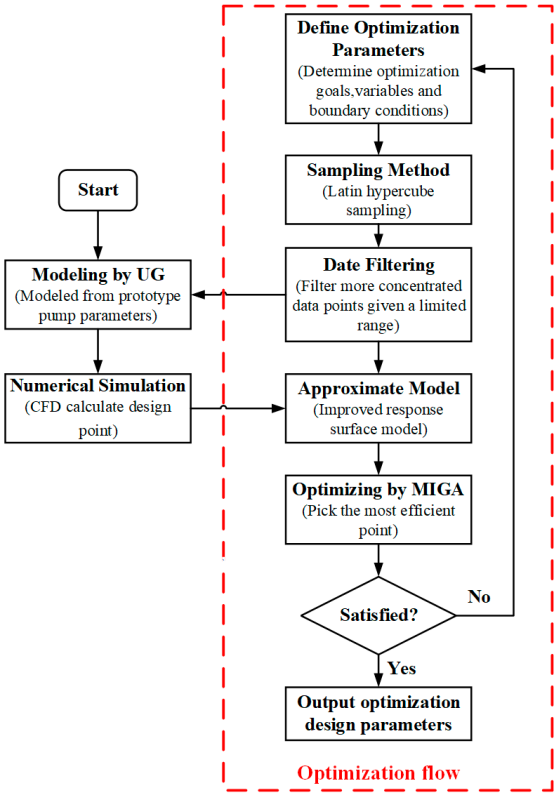

Figure 6. Optimization flow chart.

3.1. Optimization Objective

Due to the long-term and continuous operation of the pump and its frequent operation under low load or variable load, the operating point of the pump easily deviates from the high-efficiency area; the operating efficiency of the pump is then greatly reduced, and a large amount of energy is wasted. In order to save energy and reduce the internal energy loss so as to improve the operating efficiency of the two-stage split centrifugal pump, this paper takes the efficiency at the design operating point as the optimization goal. The efficiency equation is as follows:

$$\eta = \frac{Q}{3600} \times \frac{p_{2t} - p_{1t}}{T \times \omega} \tag{2}$$

where Q is the flow rate at the design operating point (m^3/h); p_{2t} and p_{1t} are the total pressure at the inlet and outlet, respectively (Pa); T is the torque of the impeller (N m); and ω is the rotational speed of the impeller (rad/s).

3.2. Design Variables and Parameter Ranges

Since this paper only addresses the design and optimization of the blade profile, in order to reduce the complexity and error of the overall calculation, the diameter of the impeller inlet and outlet and the thickness of the blade were kept unchanged. There were nine design variables to be optimized and controlled, and the range of each design variable is shown in Table 4. In the table, x_1 represents the outlet width of the blade, which is used to control the variation range of the size of the impeller on the axial projection diagram. x_2 and x_3 represent the inlet placement angles of the rear and front cover plates of the blade, respectively, while x_4 and x_5 represent the outlet placement angles of the rear and front cover plates of the blade, respectively. The blade wrap angle was set as the design variable x_6; variable x_7 is the Stepanoff number that controls the change of the cross-sectional area in the volute; x_8 and x_9 represent the volute inlet width and the starting position of the volute baffle, respectively.

Table 4. Boundary range of design parameters.

Design Parameter	Lower Limit	Upper Limit
x_1	10	20
x_2	25	35
x_3	20	30
x_4	20	30
x_5	20	30
x_6	115	135
x_7	0.15	0.3
x_8	70	90
x_9	150	180

3.3. Latin Hypercube Sampling Method

As an important step in the optimization process of an experimental design, it is necessary to choose an appropriate sampling technique. Since there are many variables in this optimization design, in order to obtain better space-filling randomness, accuracy, and robustness for the sample parameters, the LHS method was used to generate 149 sets of valid data for the defined nine variables and the range of the design variables. In order to further reduce the error of the sample and obtain more concentrated data sample points, thereby improving the convergence and fitting accuracy of the data, corresponding thresholds were set for the head and efficiency in the sample data. The threshold of the head was set to 135 m and the threshold of efficiency to 78%. Finally, three partial data sets, as shown in Figure 7, were screened out. Namely, zone 1 represents data that exceeds the efficiency threshold; zone 2 represents data within the set efficiency and head thresholds; zone 3 represents data that exceeds the head threshold. The 99 groups of valid data screened in the zone 2 were selected for subsequent model training and prediction.

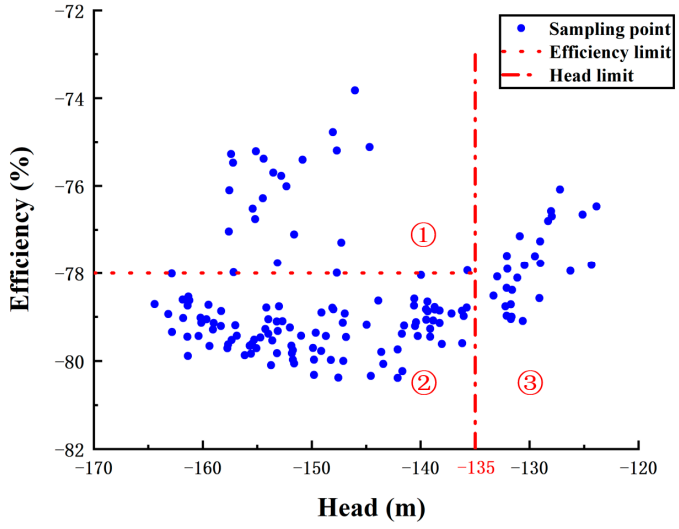

Figure 7. Sample data screening diagram.

3.4. Non-Hierarchical Response Surface Methodology

As a common approximation model established between the objective function and the design variables, RSM has multiple selectable polynomial orders, such as first- (linear), second-, third-, and fourth-order polynomial functions. Based on the multi-parameter optimization design in this paper, in order to improve the accuracy of the model prediction

results, the fourth-order RSM was selected for the fitting calculations. The fourth-order RSM polynomial function is expressed as follows:

$$f(x) = a_0 + \sum_{i=1}^{n} b_i x_i + \sum_{ij(i<j)} c_{ij} x_i x_j + \sum_{i=1}^{n} d_i x_i^2 + \sum_{i=1}^{n} e_i x_i^3 + \sum_{i=1}^{n} g_i x_i^4 \quad (3)$$

where $x = (x_1, x_2, \ldots, x_n)$, x_i $(i = 1, 2, \ldots, n)$ are design variables, $a_0, b_i, c_{ij}, d_i, e_i, g_i$ are the regression coefficients of each polynomial, and the number of hierarchical polynomials is $1 + 9 + (81 - 9)/2 + 9 + 9 + 9 = 73$. The non-hierarchical RSM was selected to be able to use non-hierarchical polynomials in analyzing and verifying the accuracy of the model.

3.5. Optimization Algorithm

As an improved genetic algorithm based on the traditional genetic algorithm, MIGA is a pseudo-parallel genetic algorithm based on population grouping. The function of diversity and the prevention of premature maturity solve the problem experienced by traditional genetic algorithms, which are prone to falling into local optima [23,24].

Based on the 99 groups of sample data obtained by screening the original data, the above-mentioned fourth-order RSM polynomial function was used to establish the relationship between the optimization objective and the design variables; the MIGA was then used for optimization, and the performance of the impeller was finally verified. The parameter settings of the optimization algorithm are shown in Table 5.

Table 5. The parameter settings of the optimization algorithm.

Option	Value
Sub-population size	10
Number of islands	10
Number of generations	50
Rate of crossover	1.0
Rate of mutation	0.01
Elite size	1
Rel tournament size	0.5
Penalty multiplier	1000
Penalty exponent	2
Default variable bound	1000
Max failed runs	5

4. Results

4.1. Approximate Model Fit Accuracy

In order to verify the accuracy of the approximate model, this paper compares the model prediction accuracy of the third-order and fourth-order RSM polynomials in the hierarchical and non-hierarchical models. The R^2 value is used to represent the degree of agreement between the approximate model and the sample points. The closer the value is to 1, the higher the prediction accuracy of the approximate model. For the fourth-order RSM polynomial, the number of polynomials when layered is 73, and for the third-order RSM polynomial, the number of polynomials when layered is 64. Figure 8a,b present the corresponding R^2 values of the third-order and fourth-order polynomials under the hierarchy. It can be seen that the R^2 value is higher under the third-order hierarchical fitting, and the fitting effect is better. Figure 8c,d present the R^2 values corresponding to third-order and fourth-order non-hierarchical polynomials. In this optimization process, the cross-validation method was used for error analysis, and 50 groups of random data were selected for cross-validation error analysis. At the same time, automatic three-dimensional modeling and numerical simulation were performed on these 50 groups of data, and the

corresponding calculation results were finally obtained. After many instances of repeated training, it can be seen that the fitting effect of the fourth-order non-hierarchical model is better than that of the third-order model, and the fitting accuracy of non-hierarchical model is higher than that of the hierarchical model.

In this model verification, when the fourth-order model is non-hierarchical, and when the number of polynomials selected is 40, a higher fitting accuracy can be obtained. Table 6 shows the design variable values before and after optimization. The efficiency of the optimal scheme is 80.939%, which is 4.427% higher than the 76.512% before optimization. The efficiency value verified by CFD is 80.229%, and the relative error is 0.88%. Therefore, the optimization model has good reliability and can be accurately used for pump performance prediction.

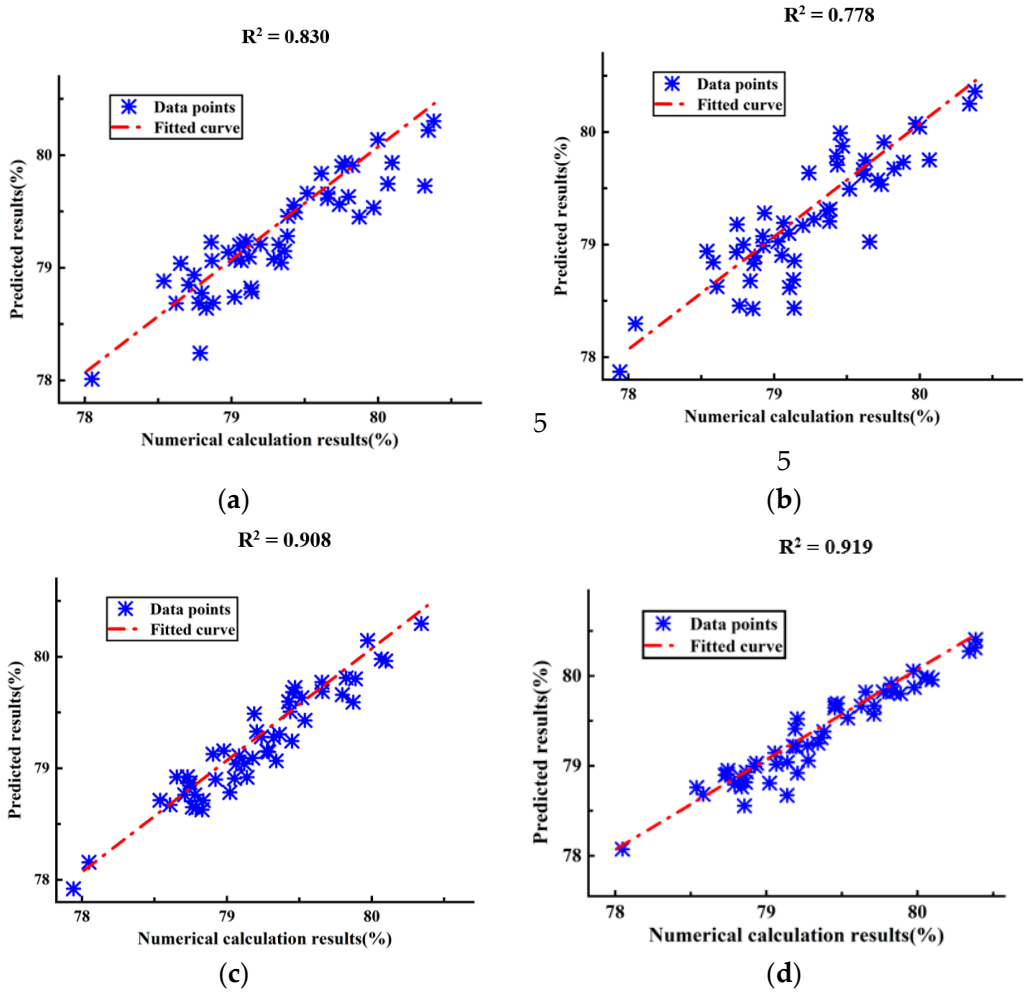

Figure 8. Corresponding values of R^2 for polynomials: cubic hierarchy (**a**), quartic hierarchy (**b**), cubic non-hierarchy (**c**), quartic non-hierarchy (**d**).

Table 6. Design variable values before and after optimization.

Variables	b_2/mm	β_{1h}/°	β_{2h}/°	β_{1s}/°	β_{2s}/°	φ/°	K_s	b_3/mm	θ/°
Original	15	33.82	25.38	25.53	25.15	124	0.2982	70	190
Optimal	14.74	32.58	26.15	20.03	26.58	127.74	0.1992	70.01	165.32

4.2. Sensitivity Analysis

In order to verify the influence of the design variables on the performance and efficiency of the pump, a sensitivity analysis was carried out for the nine variables in the optimal design. Table 7 shows the corresponding coefficient values of each polynomial using the fourth-order non-hierarchical fortieth-degree polynomial. It can be seen from the table that the coefficients of x_1, x_4, x_6, x_8, and x_9 are negative numbers; that is, the blade outlet width b_2, the blade front cover inlet placement angle β_{1s}, the blade wrap angle φ, the volute outlet width b_3, and the double-volute starting position θ of the diaphragm have a negative effect on the overall efficiency of the pump. The blade wrap angle φ and the starting position θ of the diaphragm of the double volute have a significant impact on the hydraulic power of the pump. The blade outlet width, the blade front cover inlet placement angle, and the volute outlet width have little influence on the overall performance of the pump and can almost be ignored. Because the coefficients of x_3 and x_7 are positive values, the outlet placement angle β_{2h} of the rear cover plate of the blade and the Stepanoff number K_s have a positive impact on the overall efficiency of the pump, with the Stepanoff number K_s having a greater influence. The influence of the placement angle β_{2h} at the outlet of the rear cover plate of the blade is small.

Table 7. Corresponding coefficients for each polynomial.

Term	Coefficient	Term	Coefficient	Term	Coefficient	Term	Coefficient
x_1	-9.82	${x_4}^2$	1.98×10^{-3}	x_2x_8	-3.43×10^{-3}	${x_6}^3$	-0.04
x_3	0.38	${x_6}^2$	7.26	x_3x_6	-1.20×10^{-3}	${x_7}^3$	2.54×10^{4}
x_4	-0.49	${x_7}^2$	-9.13×10^{3}	x_3x_7	0.19	${x_8}^3$	-1.56×10^{-4}
x_6	-612.25	${x_8}^2$	3.61×10^{-2}	x_3x_8	-1.82×10^{-3}	${x_9}^3$	-4.11×10^{-3}
x_7	1418.98	${x_9}^2$	1.01	x_4x_6	1.60×10^{-3}	${x_1}^4$	1.07×10^{-3}
x_8	-2.79	x_1x_7	2.28	x_4x_7	0.22	${x_2}^4$	-5.70
x_9	-111.13	x_1x_8	-4.20×10^{-3}	x_7x_9	-0.09	${x_6}^4$	7.52
${x_1}^2$	1.19	x_1x_9	3.00×10^{-3}	x_8x_9	1.06×10^{-3}	${x_7}^4$	-2.67×10^{4}
${x_2}^2$	-0.10	x_2x_4	3.71×10^{-3}	${x_1}^3$	-0.06	${x_9}^4$	6.23
${x_3}^2$	-2.41×10^{-3}	x_2x_7	0.25	${x_2}^3$	4.49×10^{-3}	*const*	2.40×10^{4}

4.3. Inner Flow Analysis

Figure 9 presents a comparison of the impeller inlet peripheral speed before and after optimization. The inlet peripheral speed of the impeller has an important influence on the pump head. If the peripheral speed is too large, it easily forms a prewhirl at the inlet and affects the impeller head. In the steady calculation, due to the uneven distribution of the dual-inlet flow channels and the water suction chamber, the inter-stage flow channels of the second-stage impeller have a great influence on the flow distribution. Under the centrifugal force of the first-stage impeller, the overall increase in the velocity distribution of the second-stage impeller is higher than that of the first-stage impeller. Compared with that before optimization, the peripheral velocity distribution of the first-stage impeller inlet shows almost no great change. After optimization, the average circumferential speed at the inlet of the second-stage impeller is 4.45 (m s^{-1}), and the average circumferential speed of the second-stage impeller inlet of the original scheme is 6.14 (m s^{-1}). Thus, compared with the original model, the overall prewhirl of the impeller inlet is reduced, therefore significantly improving the hydraulic performance of the impeller and the optimized second-stage impeller.

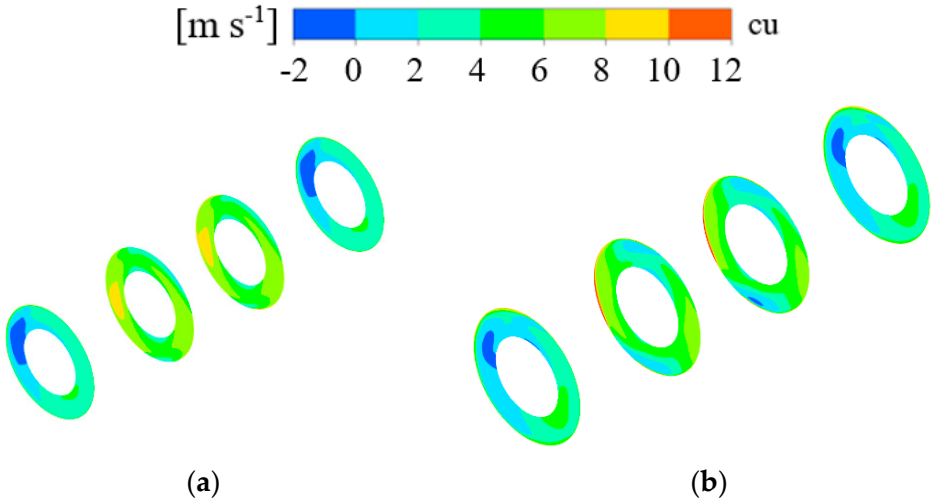

Figure 9. Comparison of the peripheral speed distribution of the impeller inlet before (**a**) and after (**b**) optimization.

Figures 10 and 11 present a comparison of the speed distribution before and after the optimization of the first-stage impeller and the second-stage impeller, respectively. It can be seen from the figures that the internal flow of the first-stage impeller of the original scheme fits better with the blade profile, while the hydraulic performance of the optimized first-stage impeller is not improved to a certain extent, but flow separation occurs in two of the flow channels. For the optimized second-stage impeller, the internal flow of the second-stage impeller of the original scheme is smooth overall, and the streamlines in the other optimized flow channels show no obvious change; however, there is a backflow phenomenon in the upper flow channel, which results in a vortex.

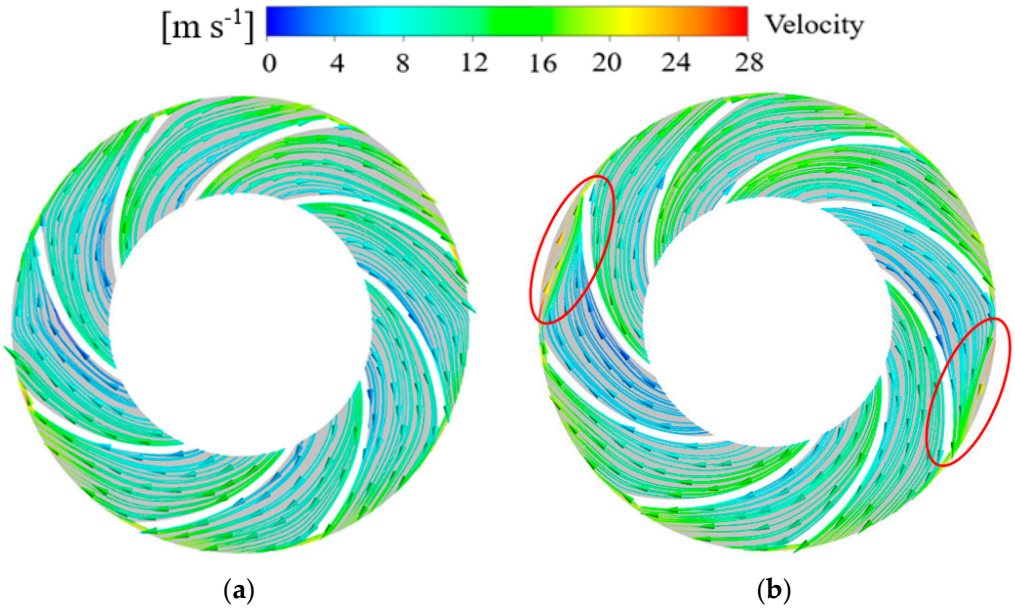

Figure 10. Comparison of the first-stage impeller velocity distribution before (**a**) and after (**b**) optimization.

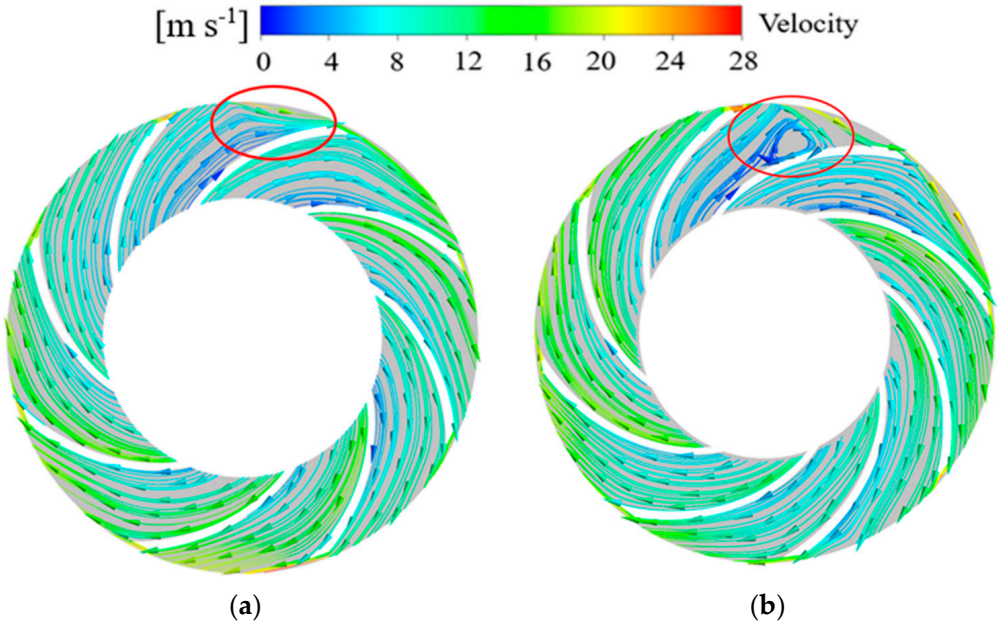

Figure 11. Comparison of the second-stage impeller velocity distribution before (**a**) and after (**b**) optimization.

Figure 12 presents a comparison of the distribution of the velocity streamlines of the double volute before and after optimization. It can be seen from the figure below that the velocity of the volute after optimization is significantly improved, the vortex at the volute and the outlet pipe is eliminated, and the impact loss at the volute tongue is eliminated. The overall velocity inside the volute is reduced, so the overall hydraulic performance of the volute is improved. Since the volute is a static water-passing component, we generally think that it has little effect on the pump's efficiency. However, as an energy-recovery component that converts kinetic energy into pressure energy, the volute has a considerable impact on the efficiency of the pump. Therefore, an improvement of the internal flow performance of the volute can effectively improve the overall operating efficiency of the pump [25].

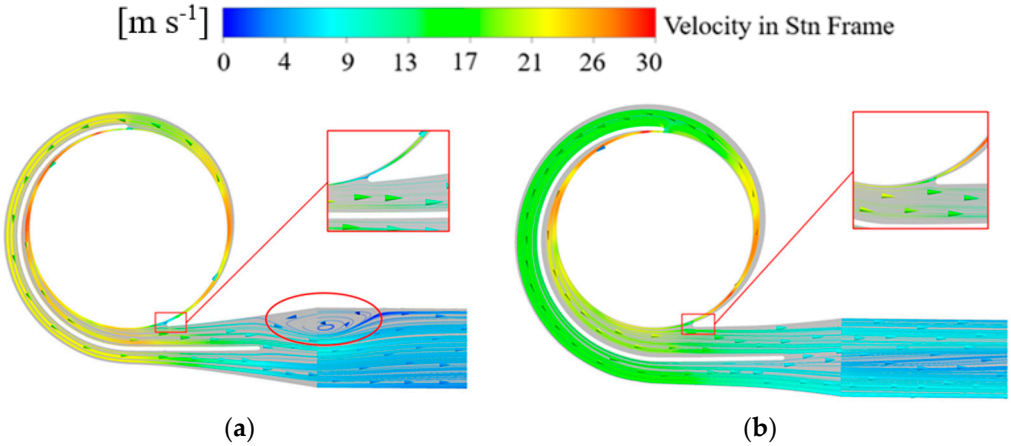

Figure 12. Comparison of the velocity streamline distribution of the double volute before (**a**) and after (**b**) optimization.

4.4. Characteristic Analysis of the Entropy Field

Due to the phenomena of secondary flow, backflow, pressure pulsation, and flow separation that aggravate energy dissipation during pump operation, energy dissipation can be effectively evaluated by comparing the entropy production results before and after

optimization. For this analysis of entropy production, the inclusion of wall dissipation, turbulent dissipation, and direct dissipation is considered based on the Reynolds time-averaged turbulent motion.

Table 8 shows the entropy production values corresponding to the wall, turbulence, and direct dissipation of different components before and after optimization, where Imp 1st1 represents the first-stage impeller on the left side of Figure 1, Imp 1st2 is the first-stage impeller on the right side, Vol is the double volute, and Imp 2nd is the second-stage impeller. It can be seen from the table that the entropy production of various dissipations of the optimized first-stage impeller is increased, and the wall dissipation of the second-stage impeller is reduced to a certain extent. The dissipation of the volute in all three parts is reduced, mainly concentrated in the dissipation of the wall, which is reduced by 9.07 (W/K) as compared with that before optimization.

Figure 13 presents a comparison chart of the entropy production results of the first-stage impeller, the second-stage impeller, and the double volute before and after optimization. As can be seen from the figure, due to the optimization of the structure of the double volute, the entropy production value after optimization is reduced by 9.64 (W/K), and the energy dissipation of the volute is significantly reduced. The other parts may have a small increase in entropy production due to the deterioration of the optimized flow state, but the overall entropy production of the pump is decreased by 4.79 (W/K). Hence, the overall energy loss of the pump is reduced, the performance is improved, and the optimization effect of the volute is better than that of the impeller.

Table 8. Entropy production for the wall, turbulence, and direct dissipation of different components before and after optimization.

	Original			**Optimization**		
Dissipation type	Wall	Turbulence	Direct	Wall	Turbulence	Direct
Imp 1st1	12.12	2.32	2.04	12.44	3.01	2.77
Imp 1st2	12.13	2.32	2.04	12.29	3.05	2.82
Vol	35.25	7.82	0.60	26.18	7.18	0.67
Imp 2nd	23.95	5.53	4.57	23.84	6.34	5.32

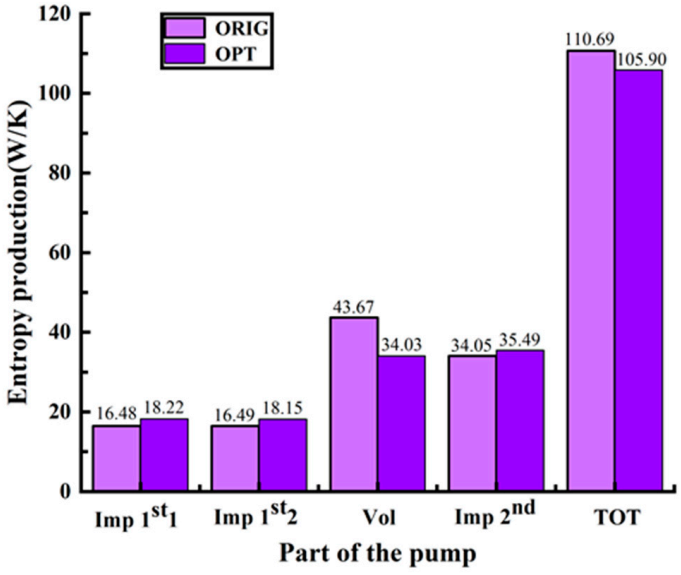

Figure 13. Comparison of entropy field values of components before and after optimization.

5. Conclusions

In this paper, the efficiency of a multi-stage double-suction pump under its design conditions was selected as the optimization target, and nine design parameters were used as the optimization variables. The LHS method was used to sample and screen the data based on the improved RSM in order to optimize the efficiency. Finally, the MIGA was used for global optimization, and the hydraulic performance of the pump before and after optimization was compared and analyzed.

(1) The non-hierarchical RSM selected in this paper, namely the fourth-order fortieth-degree non-hierarchical polynomial, can effectively approximate the nonlinear relationship between the optimization target efficiency and the design variables. The fitted R^2 value was 0.919, which was significantly improved compared with the fourth-order hierarchical polynomial and met the accuracy requirements. The efficiency under the design case after the final numerical verification was increased by 3.717%.

(2) For the fourth-order fortieth-degree hierarchical polynomial selected in this paper, the degree of influence of each variable on the efficiency can be obtained through the coefficients of each polynomial, among which the blade front cover inlet placement angle β_{1s}, the baffle starting position θ, and the blade wrap angle φ were found to have a greater impact on the efficiency, while the other variables were found to have less impact.

(3) The internal flow of the optimized double volute was well improved, eliminating the large-area vortex phenomenon in the low-pressure area at the outlet of the volute. The overall velocity inside the volute was reduced, therefore converting kinetic energy into pressure energy to a greater extent, and the energy loss was reduced.

(4) By comparing and analyzing the entropy production value of each component before and after optimization, it can be concluded that the total entropy production of the pump is reduced by 4.79 (W/K) as compared with that before optimization, while the optimized double volute entropy production is reduced by 9.64 (W/K). This is mainly due to the reduction in the wall surface entropy generation as well as the dissipation value in the double volute, which effectively reduces the energy loss of the pump and improves the overall operating performance of the pump.

Author Contributions: Conceptualization, J.P. and W.W.; methodology, W.W.; software, W.W. and J.S.; validation, J.L., J.Z. and J.W.; formal analysis, W.W.; data curation, W.W.; writing—original draft preparation, J.S.; writing—review and editing, J.P., J.L. and J.W. All authors have read and agreed to the published version of the manuscript.

Funding: This research was funded by the Natural Science Foundation of Jiangsu Province (Grant No. BK20190851), Natural Science Foundation of China (Grant No. 51879121), Primary Research and Development Plan of Jiangsu Province (Grant No. BE2019009-1), and Ranking the Top of the List for Science and Technology Projects of Yunnan Province (Grant No. 202204BW050001).

Institutional Review Board Statement: Not applicable.

Informed Consent Statement: Informed consent was obtained from all subjects involved in the study.

Data Availability Statement: Not applicable.

Conflicts of Interest: The authors declare no conflict of interest.

References

1. Osman, M.; Wang, W.; Yuan, J.; Zhao, J.; Wang, Y.; Liu, J. Flow Loss Analysis of a Two-stage Axially Split Centrifugal Pump with Double Inlet under Different Channel Designs. *Proc. Inst. Mech. Eng. Part C-J. Mech. Eng. Sci.* **2019**, *233*, 5316–5328. [CrossRef]
2. Zhang, X.; Huang, H. Flow Field Analysis of Multi-stage Middle-open Centrifugal Pump Inter-stage Flow Passage. *E3S Web Conf.* **2020**, *155*, 01014. [CrossRef]
3. Wang, W.; Osman, M.; Pei, J.; Gan, X.; Yin, T. Artificial Neural Networks Approach for a Multi-Objective Cavitation Optimization Design in a Double-Suction Centrifugal Pump. *Processes* **2019**, *7*, 246. [CrossRef]
4. Ji, Y.; Yang, Z.; Ran, J.; Li, H. Multi-objective Parameter Optimization of Turbine Impeller Based on RBF Neural Network and NSGA-II Genetic Algorithm. *Energy Rep.* **2021**, *7*, 584–593. [CrossRef]

5. Chen, J.; Wu, G. Kriging-assisted Design Optimization of the Impeller Geometry for an Automotive Torque Converter. *Struct. Multidiscip. Optim.* **2018**, *57*, 2503–2514. [CrossRef]
6. Piri, J.; Pirzadeh, B.; Keshtegar, B.; Givehchi, M. Reliability Analysis of Pumping Station for Sewage Network Using Hybrid Neural Networks-genetic Algorithm and Method of Moment. *Process Saf. Environ. Prot.* **2021**, *145*, 39–51. [CrossRef]
7. Nataraj, M.; Singh, R.R. Analyzing Pump Impeller for Performance Evaluation Using RSM and CFD. *Desalination Water Treat.* **2014**, *52*, 6822–6831. [CrossRef]
8. Yang, P.; Chen, H.; Liu, Y. Application of Response Surface Methodology and Desirability Approach to Investigate and Optimize the Jet Pump in a Thermoacoustic Stirling Heat Engine. *Appl. Therm. Eng.* **2017**, *127*, 1005–1014. [CrossRef]
9. Alawadhi, K.; Alzuwayer, B.; Mohammad, T.; Buhemdi, M. Design and Optimization of a Centrifugal Pump for Slurry Transport Using the Response Surface Method. *Machines* **2021**, *9*, 60. [CrossRef]
10. Puttige, A.; Andersson, S.; Ostin, R.; Olofsson, T. Application of Regression and ANN Models for Heat Pumps with Field Measurements. *Energies* **2021**, *14*, 1750. [CrossRef]
11. Deng, L.; Cai, C.S. Bridge Model Updating Using Response Surface Method and Genetic Algorithm. *J. Bridge Eng.* **2010**, *15*, 553–564. [CrossRef]
12. Khairy, E.; Chris, L. Optimization of the Cyclone Separator Geometry for Minimum Pressure Drop Using Mathematical Models and CFD Simulations. *Chem. Eng. Sci.* **2010**, *65*, 6048–6058. [CrossRef]
13. Miletic, T.; Ibric, S.; Duric, Z. Combined Application of Experimental Design and Artificial Neural Networks in Modeling and Characterization of Spray Drying Drug: Cyclodextrin Complexes. In Proceedings of the 14th Chinese Drying Conference (CDC), Changzhou, China, 11–14 October 2013; Volume 32, pp. 167–179. [CrossRef]
14. Wang, X.; Zhang, B.; Tan, L.; Zhai, J.; Cao, S. Development of a Pump-turbine Runner Based on Multiobjective Optimization. In Proceedings of the 27th IAHR Symposium on Hydraulic Machinery and Systems (IAHR), Montreal, QC, Canada, 22–26 September 2014; Volume 22. [CrossRef]
15. Zhang, H.; Gao, X.; Sun, B.; Qin, Z.; Zhu, H. Parameter Analysis and Performance Optimization for the Vertical Pipe Intake-outlet of a Pumped Hydro Energy Storage Station. *Renew. Energy* **2020**, *162*, 1499–1518. [CrossRef]
16. Ciarrocchi, E.; Arteconi, A.; Zheng, X.; Polonara, F.; Wang, R. Assessment of the Energy Performance of an Air Source Heat Pump by Response Surface Methodology. *Energy Procedia* **2017**, *105*, 439–444. [CrossRef]
17. DeLoach, R. The Role of Hierarchy in Response Surface Modeling of Wind Tunnel Data. In Proceedings of the 48th AIAA Aerospace Sciences Meeting Including the New Horizons Forum and Aerospace Exposition, Orlando, FL, USA, 4–7 January 2010. [CrossRef]
18. Bao, N.; Wang, C. A Monte Carlo Simulation Based Inverse Propagation Method for Stochastic Model Updating. *Mech. Syst. Signal Process.* **2015**, *60–61*, 928–944. [CrossRef]
19. Tanaka, T.; Yamasaki, A.; Koyamada, K.; Sakamoto, N. Interactive Hierarchical RSM Applied to Parameter Optimization of Photonic Crystal Nanocavities. In Proceedings of the 13th IEEE International Symposium on Consumer Electronics, Kyoto, Japan, 25–28 May 2009; pp. 711–715. [CrossRef]
20. Huang, R.; Luo, X.; Ji, B.; Wang, P.; Yu, A.; Zhai, Z.; Zhou, J. Multi-objective optimization of a mixed-flow pump impeller using modified NSGA-II algorithm. *Sci. China Technol. Sci.* **2015**, *58*, 2122–2130. [CrossRef]
21. Wang, Y.; Pei, J.; Yuan, S.; Wang, W. Effect of Baffles in Between Stages on Performance and Flow Characteristics of a Two-Stage Split Case Centrifugal Pump. In Proceedings of the Fluids Engineering Division Summer Meeting, Waikoloa, HI, USA, 30 July–3 August 2017. [CrossRef]
22. Lin, Y.; Li, X.; Zhu, Z.; Wang, X.; Lin, T.; Cao, H. An Energy Consumption Improvement Method for Centrifugal Pump Based on Bionic Optimization of Blade Trailing Edge. *Energy* **2022**, *246*, 123323. [CrossRef]
23. Chen, H.; Ooka, R.; Kato, S. Study on Optimum Design Method for Pleasant Outdoor Thermal Environment Using Genetic Algorithms (GA) and Coupled Simulation of Convection, Radiation and Conduction. *Build. Environ.* **2006**, *43*, 18–30. [CrossRef]
24. Wang, L.; Liu, H. Parameter Optimization of Bidirectional Re-entrant Auxetic Honeycomb Metamaterial Based on Genetic Algorithm. *Compos. Struct.* **2021**, *267*, 113915. [CrossRef]
25. Dehghan, A.; Shojaeefard, M. Experimental and Numerical Optimization of a Centrifugal Pump Volute and Its Effect on Head and Hydraulic Efficiency at the Best Efficiency Point. *Proc. Inst. Mech. Eng. Part C-J. Mech. Eng. Sci.* **2022**, *236*, 4577–4598. [CrossRef]